

THE COLLAPSE OF DIFFERENTIALLY ROTATING SUPERMASSIVE STARS: CONFORMALLY FLAT SIMULATIONS

MOTOYUKI SAIJO

Department of Physics, Kyoto University, Kyoto 606-8502, Japan

Received 2003 December 8; accepted 2004 July 26

ABSTRACT

We investigate the gravitational collapse of rapidly rotating relativistic supermassive stars by means of a 3+1 hydrodynamical simulations in conformally flat spacetime of general relativity. We study the evolution of differentially rotating supermassive stars of $q \equiv J/M^2 \sim 1$ (J is the angular momentum and M is the gravitational mass of the star) from the onset of radial instability at $R/M \sim 65$ (R is the circumferential radius of the star) to the point where the conformally flat approximation breaks down. We find that the collapse of the star of $q \gtrsim 1$, a radially unstable differentially rotating star form a black hole of $q \lesssim 1$. The main reason to prevent formation of a black hole of $q \gtrsim 1$ is that quite a large amount of angular momentum stays at the surface. We also find that most of the mass density collapses coherently to form a supermassive black hole with no appreciable disk nor bar. In the absence of nonaxisymmetric deformation, the collapse of differentially rotating supermassive stars from the onset of radial instability are the promising sources of burst and quasinormal ringing waves in the Laser Interferometer Space Antenna.

Subject headings: black hole physics — gravitation — gravitational waves — hydrodynamics — instabilities — relativity — stars: rotation

1. INTRODUCTION

There is increasing evidence that supermassive black holes (SMBHs) exist at the center of all galaxies, and that they are the sources which power active galactic nuclei and quasars (Rees 1998). For example, VLBI observations of the Keplerian disk around an object in NGC4258 indicate that the central object has a mass $M \sim 2.0 \times 10^7 M_\odot$. Also, large numbers of observations are provided by the Hubble space telescope suggesting that SMBHs exist in galaxies such as M31 ($7.0 \times 10^7 M_\odot$), M87 ($3.4 \times 10^9 M_\odot$) and our own galaxy ($3.7 \times 10^6 M_\odot$) (see for example, Kormendy 2004, for a brief overview). Although evidence of the existence of SMBHs is compelling, the actual formation process of these objects is still uncertain (Rees 2001). Several different scenarios have been proposed, some based on stellar dynamics, others on gas hydrodynamics, and still others which combine the processes. At present, there is no definitive observation as yet which confirms or rules out any one of these scenarios.

Here we discuss the collapse of a supermassive star (SMS) as one scenario of formation of an SMBH. This subject is also interesting from a viewpoint of general relativity, since the onset of radial instability at the mass shedding limit takes place at $J/M^2 \approx 1$ (J is the angular momentum, M is the total gravitational energy) in the uniformly rotating SMS (Baumgarte & Shapiro 1999; Shibata 2004), which is also considered as a critical threshold between formation of a stationary black hole (BH) and of a naked singularity. The BH uniqueness theorem says that a complete gravitational collapse of a body always results in a BH rather than a naked singularity, and that the final state of the BH should go into a stationary Kerr BH (e.g., Wald 1984). However there is a candidate to except this cosmic censor.

The collapse of a prolate spheroid with large semimajor axis leads to spindle singularities without an apparent horizon (Nakamura, Shapiro & Teukolsky 1988; Shapiro & Teukolsky 1991, 1992)¹. Therefore, a collapse of a star with the critical value $J/M^2 \sim 1$ may show us an interesting phenomenon in general relativity. What happens when the star of $J/M^2 \sim 1$ collapses? What is the final fate of a collapsing star of $J/M^2 \sim 1$? Numerical simulations can clearly show the answers to these questions.

The gravitational collapse of a star of $J/M^2 \sim 1$ has been investigated most of all in axisymmetric spacetime. The pioneering study in this field was made by Nakamura (1981). He set up a differentially rotating star, adding radial velocity to induce the collapse. He found that the criterion of formation of a BH apparent horizon is $J/M^2 \approx 0.95$. The following study has been done by Stark & Piran (1985, 1986). They set up a uniformly rotating $n = 1$ polytropic star and deplete 99 % of the whole pressure to induce the collapse. They found that the criterion of BH formation is $a_{\text{crit}}/M \pm 0.2$, and when the star exceeds the above value, flattened disk formed ($a_{\text{crit}}/M = 1.2$ for the case of 99 % pressure deplete). Note that $a_{\text{crit}} (\equiv J/M)$ represents the critical Kerr parameter that the collapse proceeds to a BH. Finally Shibata (2000) performed a collapse of a differentially rotating $n = 1$ polytropic star. He also depleted the pressure of the star to induce the collapse. He found that when J/M^2 is less than 0.5, a BH is formed when the rest mass is larger than the maximum mass of the pressure depleted J constant sequence. When J/M^2 is slightly less than 1, a BH formed when the rest mass is sufficiently larger than the maximum allowed mass on the pressure depleted J constant sequence. He also found,

¹ In order to prove violation of cosmic censor precisely, one might compute a global event horizon instead of an apparent horizon, which is difficult to treat numerically in dealing with a singularity.

by comparing his results from polytropic evolution and from Γ -law evolution of the hydrodynamics, that shock heating prevents the prompt collapse to a BH under the condition of $J/M^2 \sim 1$.

At the same time we have submitted our paper, several groups have also investigated the collapse of a relativistic star of $J/M^2 \sim 1$ in full general relativity. Shibata (2004) investigated the onset of radial instability of uniformly rotating stars in 2D and find that the criterion of J/M^2 is $\gtrsim 1$ in a very soft polytropic equation of state ($n \approx 3.01 - 3.05$; n is a polytropic index). Duez, Shapiro, & Yo (2004) investigated the collapse of a differentially rotating $n = 1$ polytropic star in 3D by depleting the pressure and find that the criterion of BH formation is $J/M^2 \approx 1$, and when the star exceeds the above value, the collapsing star forms a torus which fragments into nonaxisymmetric clumps. Sekiguchi & Shibata (2004) studied the collapsing star of $J/M^2 \sim 1$ in 2D with a polytropic index of $n = 1$ and 2 and find that the criterion for BH formation is determined by the central q_c ($\equiv j/m^2$; j is the specific angular momentum and m is the cylindrical mass) at the initial state of the star.

The purpose of this paper is the following threefold. The first is to verify the nature of the gravitational collapse of a differentially rotating radially unstable star from the viewpoint of cosmic censor. If we collapse a star of $J/M^2 \gtrsim 1$, we expect that the star cannot directly form a BH of $J/M^2 \gtrsim 1$ because of cosmic censor. Therefore it is important to find the main cause to prevent BH formation of $J/M^2 \gtrsim 1$. From the previous computational results, shock heating (Shibata 2000) and core bounce (Nakamura 1981; Stark & Piran 1985, 1986; Shibata 2000) are the dominant phenomena to prevent a star from forming a BH. However, all of the previous calculations have set up violent initial data sets, adding radial velocity or depleting pressure, to induce the collapse, it may cause abrupt transport of the energy. We therefore set up a mild, natural situation, that is a collapse of differentially rotating stars from the onset of radial instability, to focus on a graduate transport of the energy. Also, we compute the collapsing star in 3D to allow shock propagation or bar formation, if it occurs.

The second is to determine the final outcome of the collapse of differentially rotating SMSs. Two different types of rotation profile arises during the quasi-static evolution of the rotating star, that depends on the environment. One is a uniformly rotating star, maintained uniform rotation during the quasi-static evolution by sufficiently strong viscosity or strong magnetic field. The other is a differentially rotating star, impossible to retain uniform rotation in low viscosity and low magnetic field (even the star initially takes uniform rotation). For the collapse of a uniformly rotating SMS from the onset of radial instability, Saijo et al. (2002) studied 3D relativistic hydrodynamic simulation in the post-Newtonian gravitation and found that the collapse is coherent and that it is likely to form an SMBH with no significant bar nor disk formation. Followup computation has been performed in 2D hydrodynamics in full general relativity and found that approximately 10 % of the total mass can form a disk, while approximately 90 % of that should form a BH (Shibata & Shapiro 2002). For the differentially rotating stars, the final outcome may strongly depends on the amount and the distribution of initial angular momen-

tum, and the nature of angular momentum distribution of SMSs is largely unknown. We also do not know what path does a differentially rotating SMS take during the quasi-static evolution. When the amount of angular momentum of the star is sufficient, the star seems to follow in a quasi-static evolution up to the mass-shedding limit. New & Shapiro (2001) find in the Newtonian quasi-static evolution that bar formation is inevitable before reaching mass-shedding limit. When the amount of angular momentum of the star is not sufficient, the star seems to collapse at the onset of radial instability before reaching secular instability ($T/W \approx 0.14$ for a uniformly rotating incompressible Newtonian stars (Chandrasekhar 1969)) or mass-shedding limit. The purpose of this paper is to examine the collapse of the SMS from the onset of radial instability. When we consider the collapse of radially unstable differentially rotating stars, the final outcome has a possibility of differing from the collapse of uniform rotation because of the strong centrifugal force at the central core, which may prevent the prompt collapse. What is the final fate of the collapse? Does the star fragment due to the growth of the degree of differential rotation? Does the disk form during the collapse? Relativistic simulation can clearly answer to these questions.

Finally, it is important to probe whether the collapse of differentially rotating SMSs could be a promising source of gravitational waves. Direct detection of gravitational waves by ground based and space based interferometers is of great importance in general relativity, in astrophysics, and in cosmology (e.g., Thorne 1998). The catastrophic collapse is one of the promising sources of gravitational waves (e.g., New 2003). For a gravitational collapse of the star in a dynamical timescale, there are two main reasons that prevent a prompt collapse of the star, which should produce gravitational waves at that moment. One reason is core bounce and/or shock heating. Suppose gravitational force is balanced to the centrifugal force ($M/R^2 \sim R\Omega^2$) in Newtonian gravity. The total mass and the angular momentum ($J \sim MR^2\Omega$) are almost conserved during the collapse, assuming that gravitational radiation takes a little role during the collapse in the absence of nonaxisymmetric deformation prior to form a BH. Note that Ω is angular velocity, R is the radius. We may estimate the bounce radius of the star in a global sense as $R_{\text{bounce}} \approx M(J/M^2)^2$. Since the horizon radius is roughly the order of M , core bounce might take place for the case $J/M^2 \gtrsim 1$, which prevents violation of cosmic censor (Nakamura 1981). The other is bar formation. From the dimensional analysis, we can describe the rotational kinetic energy T and the gravitational binding energy W as $T \sim MR^2\Omega^2$ and $W \sim M^2/R$. We also accept the assumption that total mass and angular momentum are almost conserved during the collapse. We could estimate the radius of bar formation in terms of the ratio of the rotational kinetic energy to the gravitational binding energy as $R_{\text{bar}} \approx (M/R)(T/W)^{-1}(J/M^2)^2$. Since the dynamical instability for a uniformly rotating, incompressible Newtonian star sets in at $T/W \sim 0.27$ (Chandrasekhar 1969) and for relativistic gravitation as $T/W \sim 0.24 - 0.26$ (Shibata, Baumgarte, & Shapiro 2000; Saijo et al. 2001), bar formation takes place at the radius $R \sim 4M$ for the collapse of $J/M^2 \sim 1$. Therefore, we may expect that a gravitational collapse of $J/M^2 \sim 1$ is a promising source

of quasi-periodic gravitational waves.

This paper is organized as follows. In § 2 we present basic equations of our conformally flat approximation in general relativity. We demonstrate our code tests in § 3. We discuss our initial data sets and our numerical results for our catastrophic collapse in § 4. In § 5 we summarize our findings. Throughout this paper, we use geometrized units ($G = c = 1$) and adopt Cartesian coordinates (x, y, z) with the coordinate time t . Greek and Latin indices run over (t, x, y, z) and (x, y, z) , respectively.

2. 3+1 RELATIVISTIC HYDRODYNAMICS IN CONFORMALLY FLAT SPACETIME

In this section, we briefly describe the conformally flat spacetime (e.g., Isenberg & Nester 1980). We solve the fully relativistic equations of hydrodynamics, but neglect nondiagonal spatial metric components (Wilson & Mathews 1989, 1995).

2.1. The gravitational field equations

We define the spatial projection tensor $\gamma^{\mu\nu} \equiv g^{\mu\nu} + n^\mu n^\nu$, where $g^{\mu\nu}$ is the spacetime metric, $n^\mu = (1/\alpha, -\beta^i/\alpha)$ the unit normal to a spatial hypersurface, and where α and β^i are the lapse and shift. Within a first post-Newtonian approximation, the spatial metric $g_{ij} = \gamma_{ij}$ may always be chosen to be conformally flat

$$\gamma_{ij} = \psi^4 \delta_{ij}, \quad (1)$$

where ψ is the conformal factor (see Chandrasekhar 1965; Blanchet, Damour, & Schäfer 1989). The spacetime line element then reduces to

$$ds^2 = (-\alpha^2 + \beta_k \beta^k) dt^2 + 2\beta_i dx^i dt + \psi^4 \delta_{ij} dx^i dx^j. \quad (2)$$

We adopt maximal slicing, for which the trace of the extrinsic curvature K_{ij} vanishes,

$$K \equiv \gamma^{ij} K_{ij} = 0. \quad (3)$$

The gravitational field equations in conformally flat spacetime for the five unknowns α , β^i , and ψ can then be derived conveniently from the 3+1 formalism (e.g., Saijo et al. 2001).

Since the spatial metric is conformally flat, the transverse part of its time derivative vanishes. The transverse part of the evolution equation of the spatial metric therefore relates the extrinsic curvature to the shift vector,

$$2\alpha\psi^{-4}K_{ij} = \delta_{jl}\partial_i\beta^l + \delta_{il}\partial_j\beta^l - \frac{2}{3}\delta_{ij}\partial_l\beta^l. \quad (4)$$

Inserting eq. (4) into the momentum constraint equation, then, yields an equation for the shift β^i

$$\begin{aligned} \delta_{il}\Delta\beta^l + \frac{1}{3}\partial_i\partial_l\beta^l &= 16\pi\alpha J_i + \left(\partial_j \ln\left(\frac{\alpha}{\psi^6}\right)\right) \\ &\times \left(\partial_i\beta^j + \delta_{il}\delta^{jk}\partial_k\beta^l - \frac{2}{3}\delta_i^j\partial_l\beta^l\right), \end{aligned} \quad (5)$$

where $\Delta \equiv \delta^{ij}\partial_i\partial_j$ is the flat space Laplacian and $J_i \equiv -n^\mu\gamma_i^\nu T_{\mu\nu}$ is the momentum density. In the definition of J_i , $T_{\mu\nu}$ is the stress energy tensor.

The conformal factor ψ is determined from the Hamiltonian constraint

$$\Delta\psi = -2\pi\psi^5\rho_H - \frac{1}{8}\psi^5K_{ij}K^{ij}, \quad (6)$$

where $\rho_H \equiv n^\mu n^\nu T_{\mu\nu}$ is the mass-energy density measured by a normal observer.

Maximal slicing implies $\partial_t K = 0$, so that the trace of the evolution equation for the intrinsic curvature yields an equation for the lapse α

$$\Delta(\alpha\psi) = 2\pi\alpha\psi^5(\rho_H + 2S) + \frac{7}{8}\alpha\psi^5K_{ij}K^{ij}, \quad (7)$$

combined with eq. (6), where $S = \gamma_{jk}T^{jk}$.

Therefore, conformally flat gravitational field equations for the five unknowns ψ , $\alpha\psi$, β^i can be derived by eqs. (5) - (7).

2.2. The matter equations

For a perfect fluid, the energy momentum tensor takes the form

$$T^{\mu\nu} = \rho \left(1 + \varepsilon + \frac{P}{\rho}\right) u^\mu u^\nu + P g^{\mu\nu}, \quad (8)$$

where ρ is the rest-mass density, ε the specific internal energy, P the pressure, and u^μ the four-velocity.

We adopt a Γ -law equation of state in the form

$$P = (\Gamma - 1)\rho\varepsilon, \quad (9)$$

where Γ is the adiabatic index which we set $\approx 1.33 \sim 1.34$ in this paper.

In the absence of thermal dissipation, eq. (9), together with the first law of thermodynamics, implies a polytropic equation of state

$$P = \kappa\rho^{1+1/n}, \quad (10)$$

where $n = 1/(\Gamma - 1)$ is the polytropic index and κ is a constant.

From $\nabla_\mu T^{\mu\nu} = 0$ together with the equation of state (eq. [9]), we can derive the energy and Euler equations according to

$$\begin{aligned} \frac{\partial e_*}{\partial t} + \frac{\partial(e_* v^j)}{\partial x^j} &= -\frac{1}{\Gamma}(\rho\varepsilon)^{-1+1/\Gamma} P_{\text{vis}} \frac{\partial}{\partial x^i} (\alpha u^t \psi^6 v^i) \\ \frac{\partial(\rho_* \tilde{u}_i)}{\partial t} + \frac{\partial(\rho_* \tilde{u}_i v^j)}{\partial x^j} &= -\alpha\psi^6 (P + P_{\text{vis}})_{,i} - \rho_* \alpha \tilde{u}^t \alpha_{,i} \\ &+ \rho_* \tilde{u}_j \beta^j_{,i} + \frac{2\rho_* \tilde{u}_k \tilde{u}_k}{\psi^5 \tilde{u}^t} \psi_{,i}, \end{aligned} \quad (11)$$

where

$$e_* = (\rho\varepsilon)^{1/\Gamma} \alpha u^t \psi^6, \quad (13)$$

$$v^i = \frac{dx^i}{dt} = \frac{u^i}{u^t}, \quad (14)$$

$$\rho_* = \rho \alpha u^t \psi^6, \quad (15)$$

$$\tilde{u}^t = (1 + \Gamma\varepsilon) u^t, \quad (16)$$

$$\tilde{u}_i = (1 + \Gamma\varepsilon) u_i, \quad (17)$$

and v^i , P_{vis} is the 3-velocity, pressure viscosity, respectively. Note that we treat the matter fully relativistically; the conformally flat approximation only enters through simplifications in the coupling to the gravitational fields. Note also that we include an artificial viscosity, since core bounce might occur in our gravitational collapse and that should produce shocks. We will explain our form of an artificial viscosity in § 3. As a consequence to treat shocks we also need to solve the continuity equation

$$\frac{\partial \rho_*}{\partial t} + \frac{\partial(\rho_* v^i)}{\partial x^i} = 0, \quad (18)$$

separately.

We solve the matter evolution in second order accurate in space and time with the transfer scheme of van Leer (1977); Oohara & Nakamura (1989).

2.3. Numerical techniques for solving gravitational field equations

There are three key issues to solve gravitational field equations numerically. The first is to introduce symmetric tensor \hat{A}_{ij} related to the extrinsic curvature K_{ij} as (Shibata & Nakamura 1995)

$$\hat{A}_{ij} \equiv \psi^2 \left(K_{ij} - \frac{1}{3} \gamma_{ij} K \right), \quad (19)$$

$$\hat{A}^{ij} \equiv \psi^{10} \left(K^{ij} - \frac{1}{3} \gamma^{ij} K \right). \quad (20)$$

Therefore, we describe the equations of conformal factor (eq. [6]) and lapse (eq. [7]) as

$$\Delta\psi = -2\pi\psi^5 \rho_{\text{H}} - \frac{1}{8} \psi^{-7} \hat{A}_{ij} \hat{A}^{ij}, \quad (21)$$

$$\Delta(\alpha\psi) = 2\pi\alpha\psi(\rho_{\text{H}} + 2S) + \frac{7}{8} \alpha\psi^{-7} \hat{A}_{ij} \hat{A}^{ij}. \quad (22)$$

Note that the dependence value (such as ψ , $\alpha\psi$) of the source term is always lower than $O(\psi^1)$, $O((\alpha\psi)^1)$, which is safe for a convergence during the iteration.²

The second is to decompose the vector type elliptic equation. The equation for the shift,

$$\begin{aligned} \delta_{ij} \Delta\beta_j + \frac{1}{3} \partial_i \partial_l \beta^l &= \frac{2}{\psi^6} \left(\partial^j \alpha - 6 \frac{\alpha}{\psi} \partial^j \psi \right) \hat{A}_{ij} + 16\pi\alpha J_i \\ &\equiv \hat{J}_i, \end{aligned} \quad (23)$$

can be further simplified by introducing a vector P_i and a scalar η according to (Shibata 1997)

$$\Delta P_i = \hat{J}_i, \quad (24)$$

$$\Delta\eta = -\hat{J}_i x^i. \quad (25)$$

The shift can then be computed from

$$\delta_{ij} \beta^j = \frac{7}{8} P_i - \frac{1}{8} (\partial_i \eta + x^k \partial_i P_k), \quad (26)$$

and will automatically satisfy eq. (23). Next, we decompose the symmetric tensor \hat{A}_{ij} as (e.g., York 1979)

$$\hat{A}_{ij} = \hat{A}_{ij}^* + (\hat{W})_{ij}, \quad (27)$$

where

$$\partial_j \hat{A}^{*ij} = \tilde{\gamma}_{ij} \hat{A}^{*ij} = 0, \quad (28)$$

$$(\hat{W})_{ij} = \partial_i W_j + \partial_j W_i - \frac{2}{3} \delta_{ij} \partial_k W^k. \quad (29)$$

Therefore, we can rewrite the Momentum constraint as

$$\Delta W_i + \frac{1}{3} \partial_i \partial_j W^j = 8\pi\psi^6 J_i. \quad (30)$$

We also decompose the vector W^i with the same manner as the shift;

$$\delta_{ij} W^j = \frac{7}{8} B_i - \frac{1}{8} (\partial_i \chi + x^k \partial_i B_k), \quad (31)$$

² Since we compute the variabilities of the matter as ρ_* , e_* , \tilde{u}_i , the first term of eq. (21) behaves as $-2\pi\psi^{-1}(\psi^6 \rho_{\text{H}})$.

where B_i and χ satisfies

$$\Delta B_i = 8\pi\psi^6 J_i, \quad (32)$$

$$\Delta\chi = -8\pi\psi^6 J_i x^i. \quad (33)$$

Note that J_i only appears in the presence of matter, which means that the source terms of eqs. (32) and (33) are compact. Therefore, we can compute these values quite accurately.

To summarize, we have reduced Einstein equations in a conformally flat spacetime to 10 elliptic equations for 10 variables (B_i , χ , ψ , $\alpha\psi$, P_i , η),

$$\Delta B_i = 8\pi\psi^6 J_i \equiv 4\pi S_{B_i}, \quad (34)$$

$$\Delta\chi = -8\pi\psi^6 J_i x^i \equiv 4\pi S_{\chi}, \quad (35)$$

$$\Delta\psi = -2\pi\psi^5 \rho_{\text{H}} - \frac{1}{8} \psi^{-7} \hat{A}_{ij} \hat{A}^{ij} \equiv 4\pi S_{\psi}, \quad (36)$$

$$\begin{aligned} \Delta(\alpha\psi) &= 2\pi\alpha\psi(\rho_{\text{H}} + 2S) + \frac{7}{8} \alpha\psi^{-7} \hat{A}_{ij} \hat{A}^{ij} \\ &\equiv 4\pi S_{\alpha\psi}, \end{aligned} \quad (37)$$

$$\Delta P_i = 4\pi\alpha \hat{J}_i \equiv 4\pi S_{P_i}, \quad (38)$$

$$\Delta\eta = -4\pi\alpha \hat{J}_i x^i \equiv 4\pi S_{\eta}. \quad (39)$$

These Poisson-type equations are solved by imposing the following boundary condition at outer boundaries

$$B_x = -\frac{x}{r^3} \int S_{B_x} x d^3x - \frac{y}{r^3} \int S_{B_x} y d^3x + O(r^{-4}), \quad (40)$$

$$B_y = -\frac{x}{r^3} \int S_{B_y} x d^3x - \frac{y}{r^3} \int S_{B_y} y d^3x + O(r^{-4}), \quad (41)$$

$$B_z = -\frac{z}{r^3} \int S_{B_z} z d^3x + O(r^{-4}), \quad (42)$$

$$\chi = \frac{1}{r} \int S_{\chi} x^i d^3x + O(r^{-3}), \quad (43)$$

$$\psi = 1 - \frac{1}{r} \int S_{\psi} d^3x + O(r^{-3}), \quad (44)$$

$$\alpha\psi = 1 - \frac{1}{r} \int S_{\alpha\psi} d^3x + O(r^{-3}), \quad (45)$$

$$P_x = -\frac{x}{r^3} \int S_{P_x} x d^3x - \frac{y}{r^3} \int S_{P_x} y d^3x + O(r^{-4}), \quad (46)$$

$$P_y = -\frac{x}{r^3} \int S_{P_y} x d^3x - \frac{y}{r^3} \int S_{P_y} y d^3x + O(r^{-4}), \quad (47)$$

$$P_z = -\frac{z}{r^3} \int S_{P_z} z d^3x + O(r^{-4}), \quad (48)$$

$$\eta = \frac{1}{r} \int S_{\eta} x^i d^3x + O(r^{-3}). \quad (49)$$

Here we briefly explain our order of computing 10 Poisson-type equations. First, we solve B_i and χ since the source terms do not depend on other unknown space-time variables. Once we derive the symmetric tensor A_{ij} from B_i and χ , we solve ψ iteratively till the convergence. After that we solve $\alpha\psi$ iteratively till the convergence. Finally, we solve P_i and η . We use Modified Incomplete Cholesky decomposition Conjugate Gradient (MICCG) method (Murata, Natori & Karaki 1990) to solve elliptic equations.

Finally, we should maintain our grid resolution at the central core of the collapsing star. The nested grid is one of the most appropriate way to handle this problem (see,

e.g., Ruffert 1992). Our method is a mimic version of the nested grid to handle the collapsing star problem, which is based on the rigridding method of Shibata & Shapiro (2002). For the post homologous collapse of the SMS, there are two different timescales in the collapsing star; one is the collapsing timescale at the center and the other is the one at the envelope, which is sufficiently longer than that at the center. Therefore, Shibata & Shapiro (2002) add the grid number at the intermediate stage of the collapse in order to control both regions, center and envelope of the star. Since we perform the collapse of an SMS in 3D, we concentrate on the central core of the collapse due to the limitation of computational resource. In order to maintain spatial grid resolution especially at the center, we shrink the total grid to one half as the core radius of the star becomes half from the beginning of the present grid resolution. Although this method changes the boundary condition when we “zoom in” the computational domain, it is approximately good when the difference of the gravitational mass between the end of the previous computational grid and the beginning is small. In fact, the difference of the gravitational mass between every two computational domains is less than $\approx 10^{-4}$, and therefore this “zoom-in” method should behave as a reasonable approximation for a collapse of differentially rotating SMSs.

We monitor the gravitational mass M and the angular momentum J

$$\begin{aligned} M &= -\frac{1}{2\pi} \oint_{\infty} \nabla^i \psi dS_i \\ &= \int [(\rho + \rho\varepsilon + P)(\alpha u^t)^2 - P] \psi^5 \\ &\quad + \frac{1}{16\pi} \psi^5 K_{ij} K^{ij} d^3x, \end{aligned} \quad (50)$$

$$\begin{aligned} J &= -\frac{1}{2\pi} \oint_{\infty} (xK_y^i - yK_x^i) \psi^6 dS_i \\ &= \int (xJ_y - yJ_x) \psi^6 d^3x, \end{aligned} \quad (51)$$

during the evolution. In all cases reported in § 4, the gravitational mass was conserved up to $\sim 0.1\%$, and the angular momentum up to $\sim 1\%$ of their initial values.

We also compute proper mass M_p , rotational kinetic energy T , gravitational binding energy W in equilibrium as

$$M_p = \int \rho u^t (1 + \epsilon) \sqrt{-g} d^3x = \int \rho_* (1 + \epsilon) d^3x, \quad (52)$$

$$\begin{aligned} T &= \frac{1}{2} \int \Omega T_\phi^t \sqrt{-g} d^3x \\ &= \frac{1}{2} \int \Omega (xJ_y - yJ_x) \psi^6 d^3x, \end{aligned} \quad (53)$$

$$W = M_p + T - M, \quad (54)$$

where Ω the angular velocity of the star.

Since we use a polytropic equation of state at $t = 0$, it is convenient to rescale all quantities with respect to κ (Cook, Shapiro, & Teukolsky 1992). Since $\kappa^{n/2}$ has dimensions of length, we introduce the following non-dimensional variables

$$\begin{aligned} \bar{t} &= \kappa^{-n/2} t, & \bar{x} &= \kappa^{-n/2} x, & \bar{y} &= \kappa^{-n/2} y, \\ \bar{z} &= \kappa^{-n/2} z, & \bar{\Omega} &= \kappa^{n/2} \Omega, & \bar{M} &= \kappa^{-n/2} M, \\ \bar{R} &= \kappa^{-n/2} R, & \bar{J} &= \kappa^{-n} J. \end{aligned} \quad (55)$$

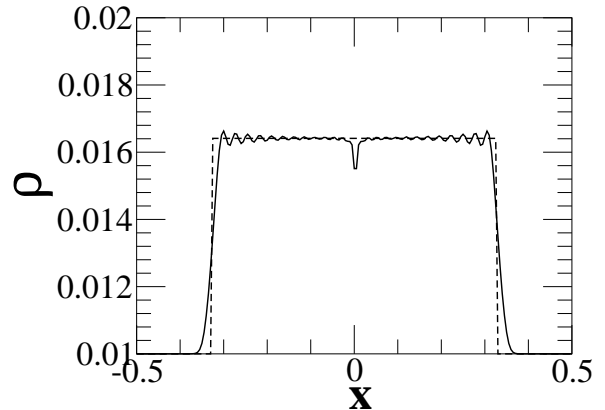


FIG. 1.— Comparison between numerical and analytical results in a one-dimensional relativistic wall shock problem at $t/M = 1.0$ (where the fluid flow is aligned with the x -axis). Solid and dashed lines represent analytic and numerical results, respectively. For this simulation we chose $\Gamma = 1.33$, $\rho^{(0)} = 1.00 \times 10^{-2}$ with a grid space $\delta x = 5 \times 10^{-3}$ and $v_0 = 0.200$.

Henceforth, we adopt nondimensional quantities, but omit the bars for convenience (equivalently, we set $\kappa = 1$).

3. CODE TESTS

First, we demonstrate 1D relativistic wall shock problem to check whether our code has an ability to treat shock. We set up the form of artificial pressure viscosity (Hawley, Smarr, & Wilson 1984) as

$$P_{\text{vis}} = \begin{cases} C_{\text{vis}} \rho^* (1 + \Gamma \epsilon) (\delta v)^2, & \text{for } \delta v \leq 0; \\ 0, & \text{for } \delta v \geq 0, \end{cases} \quad (56)$$

where $\delta v \equiv 2\delta x \partial_i v^i$, $\delta x (= \Delta x = \Delta y = \Delta z)$ is the local grid spacing and where C_{vis} is the dimensionless parameter. When evolving the matter equations we limit the stepsize Δt by the following Courant condition ($\Delta t = \min(0.3, C_{\text{dyn}} / \sqrt{\rho_{\text{max}}^*} \Delta x)$), where the second term represents dynamical time of a collapsing star. We choose the dimensionless parameter $C_{\text{dyn}} \approx 0.01$.

We have tested the ability of our code to resolve shocks by performing a wall-shock problem, in which two phases of a fluid collide. In Fig. 1 we compare numerical results with the analytic solution for initial velocities that are similar to those found in our simulations below. With $C_{\text{vis}} = 3$ we find good agreement, and set this value to simulate the catastrophic collapse in §4.

Next, we demonstrate a spherical dust collapse in Fig 2. Note that our conformally flat approximation retains all the nonlinear terms to maintain the exact dynamics for a spherical spacetime. We compare 1D and 3D results to check whether our 3D code has an ability to reproduce a spherical dust collapse. Note that we construct our 1D code following Wilson’s approach (Wilson 1979) described in Appendix A. We choose the grid size of 1D computation as 5,000, while of 3D one as $(101 \times 101 \times 51)$. We find a very good agreement of the central lapse between our 1D result and our 3D conformally flat one within the error of 1%. We terminate the integration of our 3D code at $t/M = 18.6$, since the convergence of the iteration process in our elliptic solver becomes significantly slow.

Then, we demonstrate the collapse of a spherical star in Fig. 3 (see Table 1 for an equilibrium profile). Since a

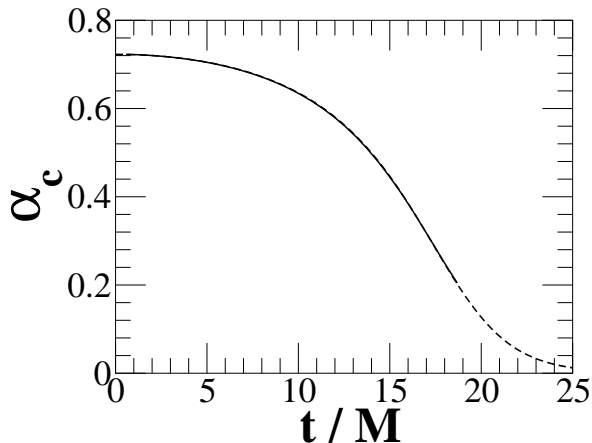


FIG. 2.— Comparison of the central lapse between three-dimensional and one-dimensional results in Oppenheimer-Snyder collapse. We start the collapse of a spherical dust from $R = 4M$. Solid and dashed lines represent the central lapse of three-dimensional and one-dimensional results, respectively.

TABLE 1
PARAMETERS FOR THE INITIAL SPHERICAL
EQUILIBRIUM SMS

ρ_0^{maxa}	R_c^{b}	M^{c}	R_c/M
3.80×10^{-6}	2.49×10^2	3.83	65.0

^aMaximum rest-mass density

^bEquatorial circumferential radius

^cGravitational mass

radially unstable spherical star only collapses to form a spherical BH promptly, we should follow the collapse of a spherical star to check whether our code has an ability to follow the collapse and to find a signal of BH formation. We set up the same grid size as we did for a spherical dust collapse, covering the star with 81 grid points across the diameter. The central lapse of the star decreases monotonically, which means a collapse of a spherical star directly forms a spherical BH. Although we terminate our integration around $\alpha_c \sim 0.1$, the fact that 1D computation of the spherical star collapse finds an apparent horizon at $\alpha_c \approx 0.11$ indicates that a BH might form.

Finally, we check the stability of a uniformly rotating star whether our code has an ability to determine the radial stability of a star. Since we determine the radial stability of a differentially rotating star in §4, we should check the sensitivity of our code to determine the critical onset of radial instability of uniformly rotating stars by comparing the results derived from the turning point method.

To assess the ability of our code to distinguish stable stars from unstable ones with rotation, we consider an equilibrium sequence of uniformly rotating stars of the fixed angular momentum J ($J/M^2 = 0.644$ at the turning point). While the turning point criterion strictly identifies the onset of secular instability, the point of onset of dynamical instability nearly coincides with the secular instability point. We adopt the polytropic index of $n = 2.96$, which is regarded as radiation pressure dominant, SMS sequence, and grid resolution as in the spherical simulations reported above. We decrease the initial

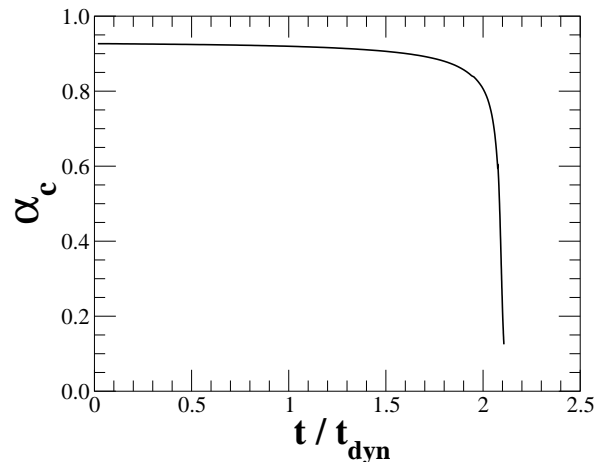


FIG. 3.— Central lapse of the spherical collapse (see Table. 1). Monotonic decrease of central lapse indicates a prompt collapse to a spherical BH.

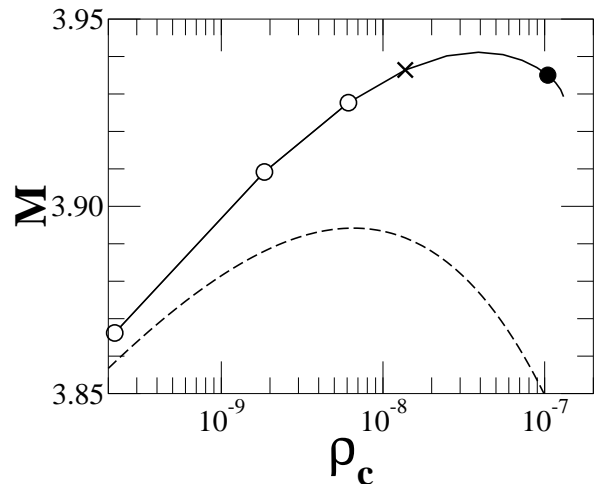


FIG. 4.— Probing the dynamical stability of a rotating SMS with $n = 2.96$, $J = 10$. Here, ρ_c is the central density of the equilibrium rotating star. Filled circles and crosses represent unstable stars, while open circles represent stable stars according to our dynamical calculation. A cross indicates that the star is actually stable analytically according to the turning point criterion. The radii of the 5 marked stars are $R/M = 254, 421, 539, 708,$ and 1579 , where the sequence starts at the right side of the figure at the highest central densities. Note that the solid line shows a constant J sequence with $J = 10$, while the dashed line represents the spherical equilibrium sequence. With the adopted grid resolution, our code can distinguish stable stars from unstable ones within 0.3% of the maximum gravitational mass.

pressure to induce the collapse ($\kappa \rightarrow 0.99\kappa$).

Figure 4 summarizes our dynamical stability analysis for the rotating SMS. We conclude that with the adopted grid resolution, our code can distinguish stable rotating stars from unstable ones within 0.3% of the maximum gravitational mass. Figure 5 shows the evolution of the central density for stable and unstable rotating stars.

4. COLLAPSE OF A DIFFERENTIALLY ROTATING SUPERMASSIVE STAR

Here we explain our initial data sets for collapsing stars. Since we are interested in a collapsing star of $J/M^2 \sim 1$, we have three requirements to construct differentially rotating equilibrium stars.

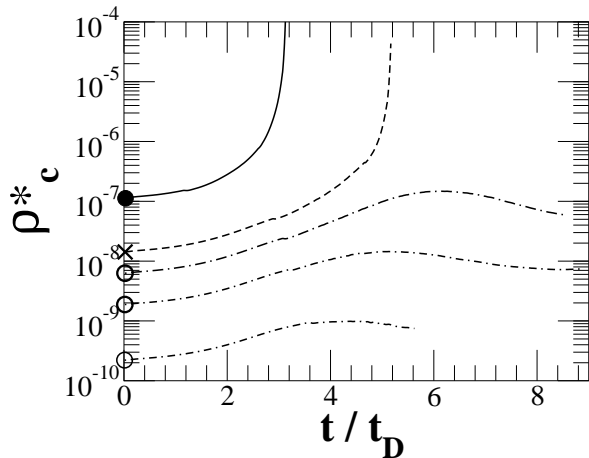


FIG. 5.— Evolution of the central densities of the stars plotted in Fig. 4. Curves are drawn for stars which are unstable both numerically and according to the turning point criterion (solid), unstable numerically but stable according to the turning point criterion (dashed), and stable both numerically and according to the turning point criterion (dash-dotted).

The first requirement is to construct radially unstable differentially rotating stars. The critical Γ to the onset of radial instability for slow rotation and weak gravitational field is described analytically as (Chandrasekhar & Lebovitz 1968; Shapiro & Teukolsky 1985)

$$\Gamma_{\text{crit}} = \frac{4}{3} + 2.25 \frac{M}{R} - \frac{2 \Omega^2 I}{9 W}, \quad (57)$$

where I is the inertia momenta of the star. Note that relativistic gravitation unstabilizes the star, while rotation, which produces centrifugal force, stabilizes the star. Although we take into account the differential rotation in the equilibrium star, this criterion (eq. [57]) may indicate the appropriate direction to choose a parameter sets of the initial condition of the rotating collapsing star. From eq. (57), we should at least choose soft equation of state to induce the collapse and set an $n = 3$ polytropic star, an SMS sequence of the star.

The second requirement is to construct a star which holds $J/M^2 \approx 1$. From the critical onset of radial instability in the equilibrium star, a uniformly rotating SMS takes the maximum of $J/M^2 \sim 0.9$ when $R/M \sim 600$ (Baumgarte & Shapiro 1999; Shibata 2004). To verify the nature of cosmic censor, we should at least go beyond $J/M^2 \gtrsim 1$. The main restriction to hold large J/M^2 comes from the mass shedding limit of the star. Therefore, to construct a star of $J/M^2 > 1$ in radially unstable branch, differential rotation of the star is required in SMS sequence.

The last requirement is high degree of differential rotation. It is indeed one path to construct high degree of differential rotation in quasi-static evolution, and reach the onset of radial instability.

To summarize, we need soft equation of state and high degree of differential rotation, and choose an $n = 3$ polytropic star (SMS sequences) and the degree of differential rotation as $\Omega_c/\Omega_{\text{eq}} \approx 10$ where we define the rotation profile as

$$u^t u_\varphi = A^2 (\Omega_c - \Omega). \quad (58)$$

In the Newtonian limit ($u^t \rightarrow 1$, $u_\varphi \rightarrow \varpi^2 \Omega$), this rotation law can be written as

$$\Omega = \frac{A^2 \Omega_c}{\varpi^2 + A^2}, \quad (59)$$

where A is the degree of differential rotation, ϖ is the cylindrical radius of the star. Since A has a dimension of length, we normalize it with a proper equatorial radius \bar{R}_e , ($A = \bar{R}_e \hat{A}$). Hereafter we choose $\hat{A} = 1/3$ to construct relatively a high degree of differential rotation. We briefly summarize our method to construct relativistic rotating equilibrium stars in Appendix B.

We summarize the parameters of our differentially rotating stars at initial in Table 2. We slightly perturb our initial equilibrium state according to

$$\rho = \rho^{(\text{equilibrium})} \left(1 + \delta^{(1)} \frac{x+y}{R_e} + \delta^{(2)} \frac{x^2 - y^2}{R_e^2} \right), \quad (60)$$

where $\delta^{(1)} = \delta^{(2)} = 10^{-3}$. We install $m = 1$ and $m = 2$ density perturbation to provide the seed for one-armed spiral and bar formation, if the physical situation should lead to unstable growth. We adopt a grid size ($201 \times 201 \times 61$), so that the star is initially covered by 161 points across the equatorial diameter. We evolve the rotating SMS up to the point at which the conformally flat approximation breaks down.

Figure 6 shows the results of radial stability in 4 differentially rotating stars. Since we do not have a tool to determine radial stability in differentially rotating stars from their equilibrium states (but for determining the criterion of secular stability in rotating stars, see Bonazzola, Frieben & Gourgoulhon (1998)), the evolution is necessary to determine its stability. The criterion to determine the radial stability is as follows. When the central density of the star grows exponentially within a few dynamical time, we determine the star radially unstable. On the other hand, when the central density of the star oscillates around its equilibrium state, we determine the star radially stable. From this criterion, Model I and II have an exponential growth of the central density that means radially unstable, while Model III and IV have maximum at several dynamical times that means radially stable.

We also show the evolution of central lapse in Fig. 7. The rapid decrease of α_c below 0.3 indicates that a BH is likely to form. Model II shows that the central lapse monotonically decreases from ~ 0.9 to ~ 0.3 . This figure shows that we can follow the collapse from the regime of Newtonian gravity ($\alpha_c \sim 0.9$) to that of relativistic gravity ($\alpha_c \sim 0.3$). On the other hand Model III shows that the central lapse oscillates around its equilibrium state, and that also means the star is radially stable.

We show the final density snapshots of the stars in the equatorial plane (Fig. 8) and in the meridional plane (Fig. 9). Even in the final snapshots of radially unstable stars, the collapse is almost axisymmetric. Also, from the snapshots in the meridional plane, the material around the rotational axes collapses faster than the surrounding material due to the strong nonlinear gravitational field.

Let us now focus on the collapsing star (Model II) to probe the final outcome. We locally define the cylindrical rest mass m , angular momentum j , specific angular

TABLE 2
PARAMETERS FOR THE INITIAL DIFFERENTIALLY ROTATING EQUILIBRIUM
SMSS

Parameter	Model I	Model II	Model III	Model IV
R_p/R_e^a	0.600	0.575	0.550	0.500
ρ_0^{\max}	3.38×10^{-6}	3.38×10^{-6}	3.38×10^{-6}	3.38×10^{-6}
R_c	3.06×10^2	3.12×10^2	3.18×10^2	3.35×10^2
Ω_c^b	1.45×10^{-3}	1.49×10^{-3}	1.53×10^{-3}	1.59×10^{-3}
Ω_{eq}^c	1.38×10^{-4}	1.42×10^{-4}	1.45×10^{-4}	1.51×10^{-4}
M	4.69	4.78	4.88	5.10
J^d	2.13×10^1	2.31×10^1	2.51×10^1	2.96×10^1
T/W^e	6.47×10^{-2}	7.02×10^{-2}	7.60×10^{-2}	8.80×10^{-2}
J/M^2	0.97	1.01	1.05	1.14
R_c/M	6.53×10^1	6.52×10^1	6.52×10^1	6.57×10^1
Stability	Unstable	Unstable	Stable	Stable

^aRatio of the polar proper radius to the equatorial proper radius

^bMaximum rest-mass density

^cEquatorial angular velocity at the surface

^dAngular momentum

^eRatio of the rotational kinetic energy to the gravitational binding energy

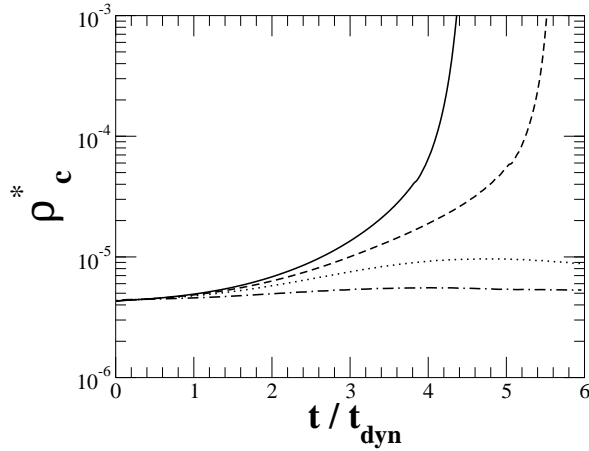


FIG. 6.— Evolution of the central density of 4 differentially rotating stars. Solid, dotted, dashed and dash-dotted line denotes Model I, II, III and IV (see Table 2)

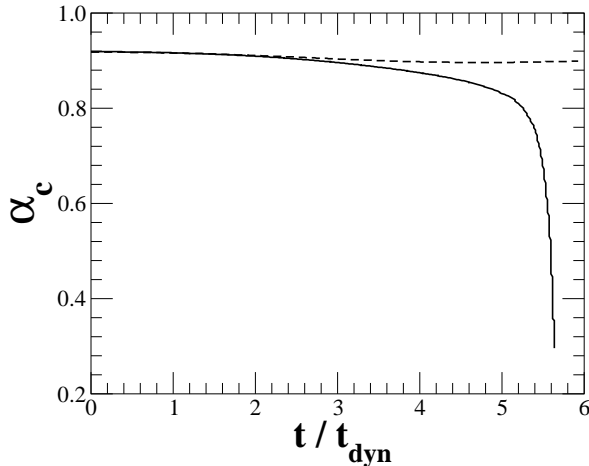


FIG. 7.— Evolution of the central lapse of 2 differentially rotating stars. Solid and dashed line denotes Model II and III, respectively (see Table 2).

momentum j_s , Keplerian angular velocity Ω_K as

$$m = 4\pi \int_0^\infty dz \int_0^\varpi d\varpi \varpi \rho^*, \quad (61)$$

$$j = 4\pi \int_0^\infty dz \int_0^\varpi d\varpi \varpi h u_\varphi, \quad (62)$$

$$j_s = 4\pi \int_0^\infty dz \int_0^\varpi d\varpi \varpi \rho^* h u_\varphi, \quad (63)$$

$$\Omega_K \equiv \sqrt{\frac{m}{\varpi^3}}, \quad (64)$$

to indicate the transport of angular momentum and the distribution of j/m^2 . We assume the axisymmetric collapse to investigate the final outcome, since the meridional density snapshots (Fig. 9) behave almost axisymmetry.

Figure 10 shows the concentration of mass density profile during the collapse. As the collapse goes on, the increase ratio of the cylindrical mass at the core of the star becomes high. In fact, 75% of the cylindrical mass is inside the radius of $r < 2M$ at $t = 5.64t_{\text{dyn}}$. We also show the mean radius, defined as $r_m = \sqrt{(\int dv \rho_* \varpi^2)/M_*}$, during the collapse in Fig. 11. Note that M_* is the rest mass. We find that the mean radius monotonically decreases, which means that the collapse of the central core is coherent.

Figure 12 shows the variation of angular velocity profile during the collapse. Since the cylindrical rest mass density shows a coherent collapse, the degree of differential rotation significantly increases at the core during the collapse and approaches to the “Keplerian” angular velocity defined in eq. (64).

We show the specific angular momentum distribution during the collapse in Fig. 13. In a global sense, J/M^2 is conserved so that a final BH should violate cosmic censor, if it forms. However, we find that most of the matter collapses to form a BH, while not a few amount of angular momentum stays at the surface area of the star that prevents forming a BH of $J/M^2 > 1$.

We show the distribution of j/m^2 in Fig. 14 during the collapse to verify cosmic censor. We find that mass

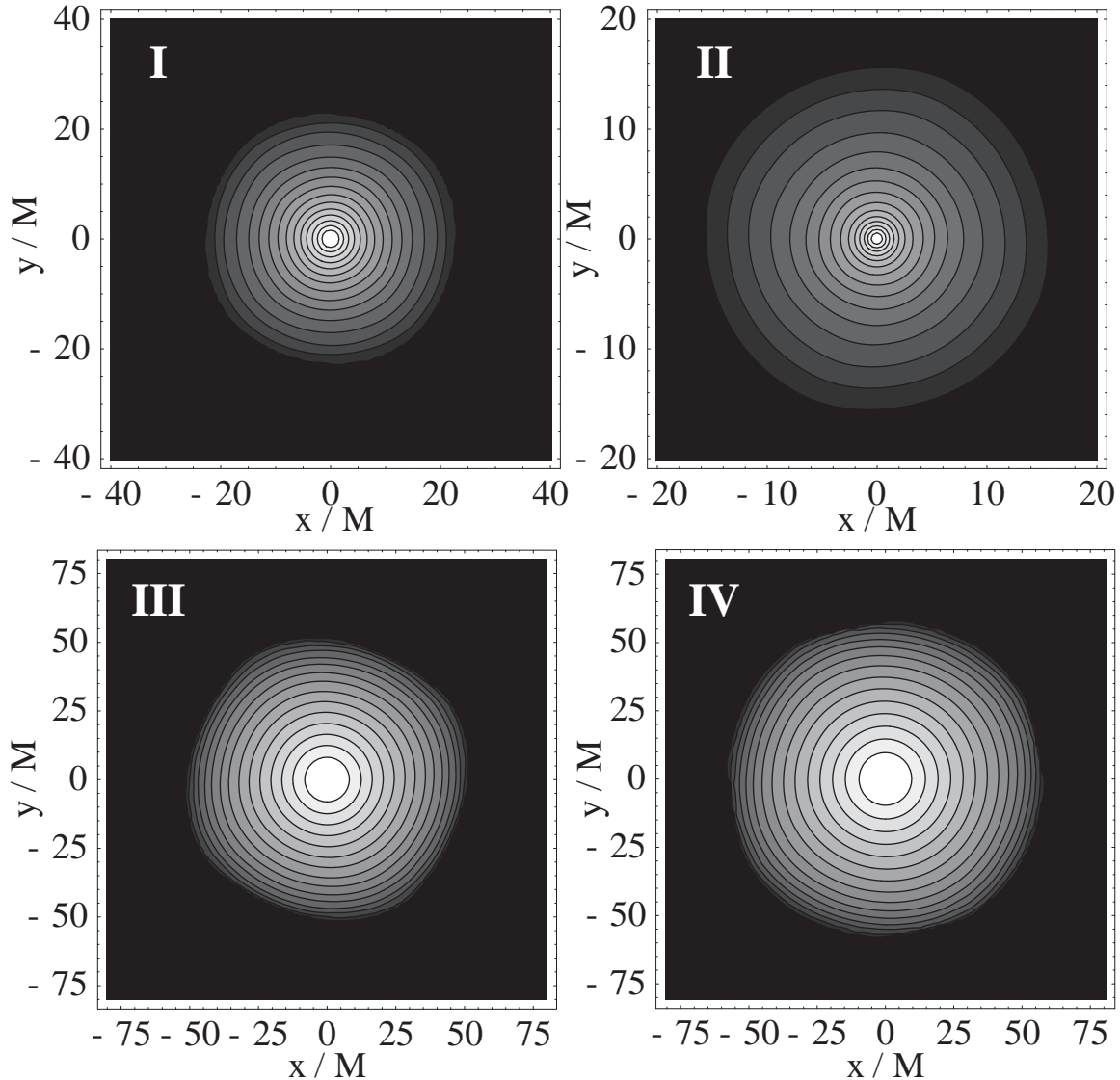


FIG. 8.— Final density contour in the equatorial plane of 4 differentially rotating stars. Model I, II, III, IV is plotted at the parameter $(t/t_{\text{dyn}}, \rho_{\text{max}}^*) = (4.38, 1.37 \times 10^{-3}), (5.62, 2.16 \times 10^{-2}), (5.61, 9.13 \times 10^{-6}), (5.60, 5.33 \times 10^{-6})$, respectively. The contour lines denote densities $\rho^* = \rho_{\text{max}}^* \times 10^{-0.267(16-i)}$ ($i = 1, \dots, 15$).

density collapses first in the central part and angular momentum remains in the surface of the star that prevents forming a BH of $J/M^2 > 1$. Note that the distribution of j/m^2 is only an indicator to interpret the physical cause to prevent BH formation. Although we should define the total gravitational mass locally to discuss the local distribution of J/M^2 , there is no knowing how to define it. Therefore we use the local rest mass instead.

5. DISCUSSION

We investigate the collapse of differentially rotating SMSs by means of hydrodynamic simulations in conformally flat approximation in general relativity. We start our collapse around the onset of radially instability at $R/M \sim 65$ to the point where conformally flat approximation breaks down.

We find that cosmic censor even holds for a gravitational collapse of a radially unstable differentially rotating equilibrium SMS of $J/M^2 \gtrsim 1$. The main reason to

prevent formation of a BH of $J/M^2 \gtrsim 1$ is that quite a large amount of angular momentum stays at the surface, not core bounce nor shock propagation, bar formation in our model. Note that even a thin disk near the surface of the star can hold relatively a large amount of angular momentum if the radius is large. The above conclusion is supported by Sekiguchi & Shibata (2004) in full general relativistic simulation that the criterion of BH formation is determined at the central $q_c (\equiv j/m^2|_{\varpi \rightarrow 0})$. In fact, the central q_c of Model II is $q_c \approx 0.89$, which satisfies their criterion.

The collapse of a differentially rotating, radially unstable SMS is coherent and likely leads to formation of an SMBH. This situation is quite similar to the collapse of a uniformly rotating SMS (e.g., Saijo et al. 2002; Shibata & Shapiro 2002), since $T/W \approx 0.08$ seems still not sufficient to change the path of the collapse from the one of uniform rotation. However, this final out-

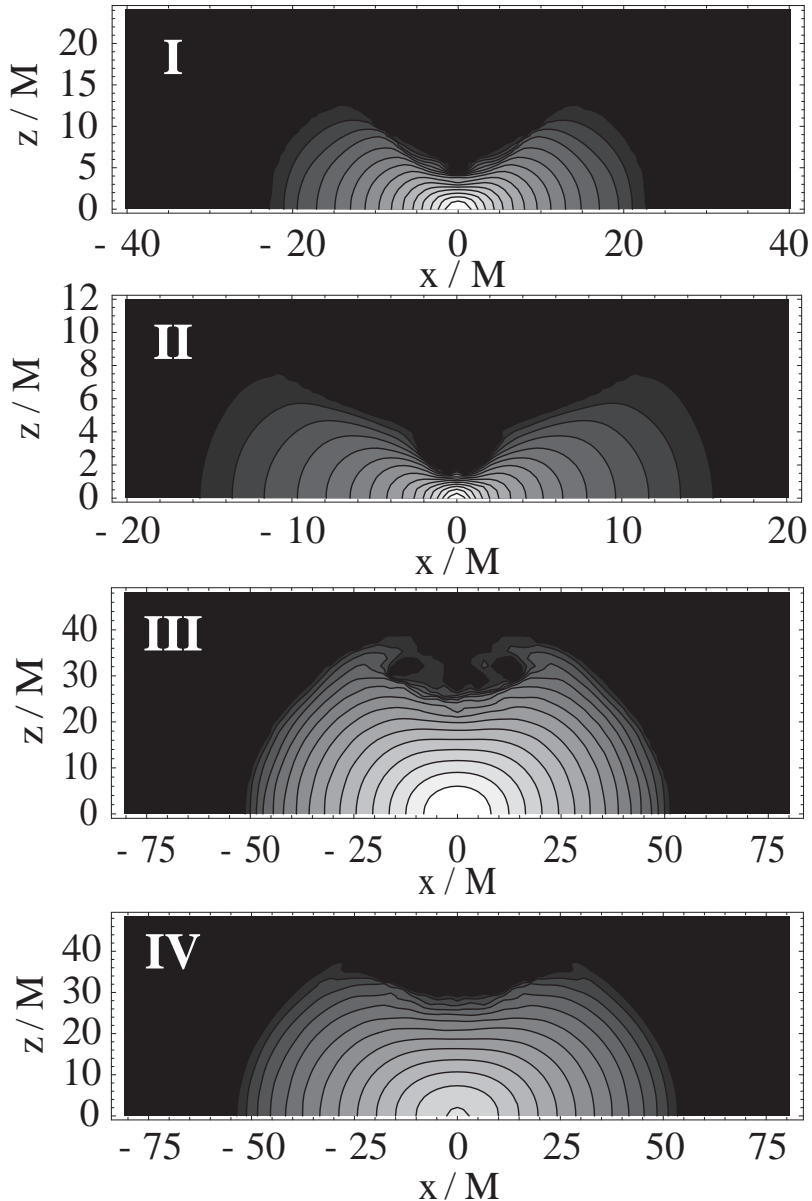


FIG. 9.— Final density contour in the meridional plane of 4 differentially rotating stars. The time and contour levels are the same as in Fig. 8.

come may depend on the equation of state of the star. Loeb & Rasio (1994) treated the isothermal ($\Gamma = 1$) collapse of initially homogeneous, uniformly rotating, low entropy clouds via smooth particle hydrodynamics (SPH) simulations. They found considerable fragmentation into dense clumps, and disk formation containing $\sim 5\%$ of the mass. They concluded that a seed BH will form at the center and that it likely will grow gradually by accretion in our model. Also Shibata (2003) treated the collapse of uniformly rotating polytropic star from the critical onset in the range of $\Gamma \approx 1.5 - 2.5$ and found that the mass of the disk is less than 10^{-3} of the gravitational mass.

We cannot find any evidence of bar formation nor significant disk formation from the rotating collapse prior to BH formation. The phenomenon of no bar formation also comes from the fact that mass density collapses first

to form a BH. In such case, T/W cannot scale in R^{-1} due to the growth of the degree of differential rotation, and as a fact the star of T/W cannot reach the dynamical instability point of ~ 0.27 . Since the $m = 1$ dynamical instability takes place when the star has a toroidal structure and soft equation of state (Centrella et al. 2001; Saijo, Baumgarte, & Shapiro 2003), we cannot find any evidence of toroidal structure at the time we stop our integration.

The rotating SMS collapse is a promising source of burst gravitational waves and of quasi-normal mode ringing waves. The characteristic frequency for burst (f_{burst}), quasi-normal mode ringing (f_{QNM}), and the wave amplitude for burst (h_{burst}), quasi-normal mode ringing

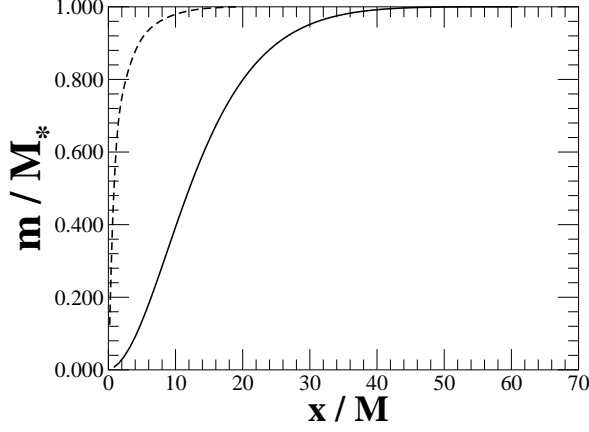


FIG. 10.— Mass density profile in the x -axes for Model II. Note that M_* is the rest mass. Solid and dashed line denotes the profile at $t = 0$ and $t = 5.64 t_{\text{dyn}}$, respectively.

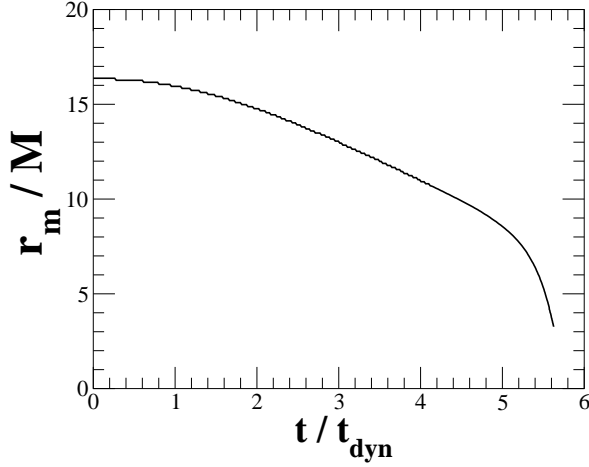


FIG. 11.— Mean radius of the star during the collapse for Model II.

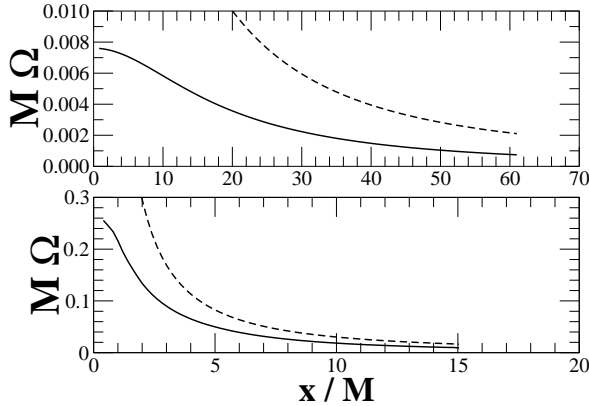


FIG. 12.— Angular velocity profile in the x -axes for Model II. Solid and dashed lines denote angular velocity of the star and Keplerian angular velocity (see eq. [64] for its definition). The top panel shows the snapshots of $t = 0$ while the bottom panel of $t \sim 5.64 t_{\text{dyn}}$.

(h_{QNM}), are (Saijo et al. 2002)

$$f_{\text{burst}} \sim 3 \times 10^{-2} \left(\frac{10^6 M_{\odot}}{M} \right) \left(\frac{M}{R} \right)^{3/2} [\text{Hz}], \quad (65)$$

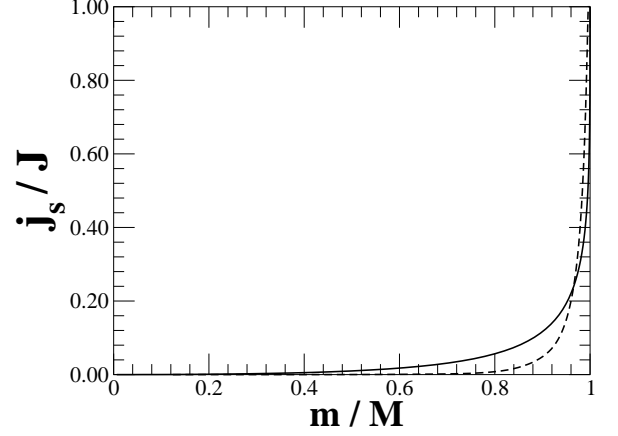


FIG. 13.— Specific angular momentum profile as a function of cylindrical mass for Model II. Solid and dashed line denotes the profile at $t = 0$ and $t = 5.64 t_{\text{dyn}}$, respectively.

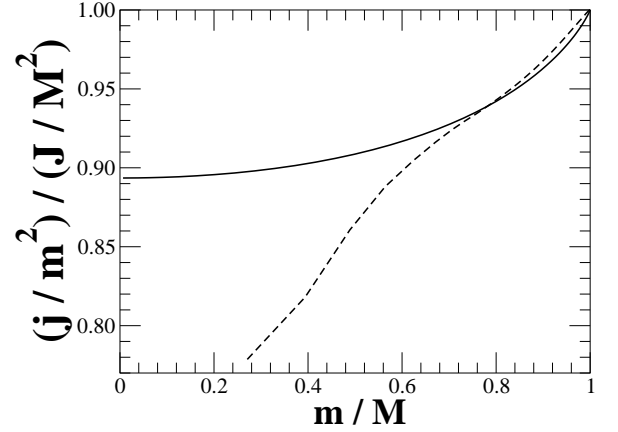


FIG. 14.— j/m^2 profile as a function of cylindrical mass for Model II. Solid and dashed line denotes the profile at $t = 0$ and $t = 5.64 t_{\text{dyn}}$, respectively.

$$h_{\text{burst}} \sim 1 \times 10^{-18} \left(\frac{M}{10^6 M_{\odot}} \right) \left(\frac{1 \text{Gpc}}{d} \right) \left(\frac{M}{R} \right), \quad (66)$$

$$f_{\text{QNM}} \sim 2 \times 10^{-2} \left(\frac{10^6 M_{\odot}}{M} \right) [\text{Hz}], \quad (67)$$

$$h_{\text{QNM}} \sim 6 \times 10^{-19} \left(\frac{\Delta E_{\text{GW}}/M}{10^{-4}} \right)^{1/2} \left(\frac{2 \times 10^{-2} [\text{Hz}]}{f_{\text{QNM}}} \right)^{1/2} \times \left(\frac{M}{10^6 M_{\odot}} \right)^{1/2} \left(\frac{1 \text{Gpc}}{d} \right), \quad (68)$$

where d is the distance from the observer and ΔE_{GW} is the total radiated energy. We set $R/M = 1$, a characteristic mean radius during BH formation. Since the main targets of LISA are gravitational radiation sources between 10^{-4} and 10^{-1} Hz, it is possible that LISA can search for the burst and quasi-normal ringing waves accompanying rotating SMS collapse and formation of an SMBH.

We would like to thank an anonymous referee for his/her critical reading of our manuscript and constructive suggestions. He also thanks Hideki Asada, Silvano Bonazzola, Ericourgoulhon, Takashi Nakamura, Ken-

ichi Nakao, Luciano Rezzolla, Stu Shapiro, Nick Streigealous, Takahiro Tanaka, Koji Uryū, Shin Yoshida for discussion. This work has been supported in part by MEXT Grant-in-Aid for young scientists (No. 200200927), Astronomical Data Analysis Center, National Astronomical Observatory of Japan, and by MEXT Grant-in-Aid for 21COE program at the Department of Physics, Kyoto

University. Numerical computations were performed on the NEC SX-5 machine in the Yukawa Institute for Theoretical Physics, Kyoto University, on the VPP-800 machine in the Academic Center for Computing and Media Studies, Kyoto University, and on the VPP-5000 machine in the Astronomical Data Analysis Center, National Astronomical Observatory of Japan.

APPENDIX

RELATIVISTIC HYDRODYNAMICS IN SPHERICALLY SYMMETRIC SPACETIME

Here we briefly explain relativistic hydrodynamics in spherically symmetric spacetime (Wilson 1979; Shapiro & Teukolsky 1980; Bowers & Wilson 1991) that we use in § 2. We can describe the line element of spherically symmetric spacetime in the isotropic coordinate as

$$ds^2 = (-\alpha^2 + \psi^4 \beta^2) dt^2 + 2\psi^4 \beta dt dr + \psi^4 (dr^2 + r^2 d\Omega), \quad (\text{A1})$$

where α is the lapse, β is the shift, ψ is the conformal factor.

We use the maximal slicing condition $K = 0$, which derives the following relation to the components of an extrinsic curvature as

$$K_r^r = -2K_\theta^\theta (= -2K_\phi^\phi). \quad (\text{A2})$$

As a consequence, we only need to consider K_r^r to construct an extrinsic curvature.

The momentum constraint derives the equation of the extrinsic curvature as

$$\frac{\partial}{\partial r} (r\psi^2 K_r^r) = (r\psi^2)^3 8\pi J_r. \quad (\text{A3})$$

The integration form of eq. (A3) is

$$K_r^r = \frac{8\pi}{(r\psi^2)^3} \int^r (r\psi^2)^3 J_r dr. \quad (\text{A4})$$

The restriction of the spatial metric to be conformally flat requires the following equation

$$2\alpha K_r^r = \frac{4}{3} r \partial_r \left(\frac{\beta}{r} \right), \quad (\text{A5})$$

which gives us an appropriate boundary condition for the extrinsic curvature as $O(r^{-3})$. Also the integration form of eq. (A5) is

$$\beta = \frac{3}{2} r \int_r \frac{\alpha K_r^r}{r} dr. \quad (\text{A6})$$

The Hamiltonian constraint and the trace of the evolution equation guide

$$\frac{1}{r^2} \partial_r (r^2 \partial_r \psi) = -2\pi \psi^5 \rho_H - \frac{3}{16} \psi^5 (K_r^r)^2, \quad (\text{A7})$$

$$\frac{1}{r^2} \partial_r [r^2 \partial_r (\alpha \psi)] = 2\pi \alpha \psi^5 (\rho_H + 2S) + \frac{21}{16} \alpha \psi^5 (K_r^r)^2, \quad (\text{A8})$$

with the boundary conditions

$$\psi = 1 + \frac{M}{2r} + o(r^{-3}), \quad (\text{A9})$$

$$\alpha \psi = 1 + \frac{M}{r} + o(r^{-3}), \quad (\text{A10})$$

at the grid edge and

$$\partial_r \alpha = \partial_r \psi = 0, \quad (\text{A11})$$

at the center ($r = 0$).

Therefore, we can determine 4 unknown variables (K_r^r , ψ , $\alpha\psi$, β) with 4 equations (eqs. [A4], [A6], [A7], [A8]).³ Matter equations can be written as

$$\frac{\partial(r^2 \rho_*)}{\partial t} + \frac{\partial(r^2 \rho_* v^r)}{\partial r} = 0, \quad (\text{A12})$$

$$\frac{\partial(r^2 e_*)}{\partial t} + \frac{\partial(r^2 e_* v^r)}{\partial r} = 0, \quad (\text{A13})$$

$$\begin{aligned} \frac{\partial(r^2 \rho_* \tilde{u}_r)}{\partial t} + \frac{\partial(r^2 \rho_* \tilde{u}_r v^r)}{\partial r} &= -r^2 \alpha \psi^6 P_{,r} - \rho_* \alpha \tilde{u}^t \alpha_{,r} \\ &+ r^2 \rho_* \tilde{u}_r \beta^r_{,r} + r^2 \frac{2\rho_* \tilde{u}_r \tilde{u}_r}{\psi^5 \tilde{u}^t} \psi_{,r}. \end{aligned} \quad (\text{A14})$$

³ We choose $\hat{A}_r^r = \psi^6 K_r^r$ instead of K_r^r from a computational point of view (See §2.3.).

We have not taken into account artificial viscosity, since shock does not seem to play an important role in a spherical dust collapse and the collapse of a spherical star. In § 3, we adopt our 1D relativistic hydrodynamic code to a spherical dust collapse by setting e_* and P_* \ll equilibrium variables of them in typical polytropic index.

We briefly mention a method to compute an apparent horizon in 1D (Shapiro & Teukolsky 1980; Nakamura, Oohara, & Kojima 1987). An apparent horizon is defined as an outermost marginally trapped surface whose future-directed outgoing null geodesics have zero expansion Θ (Hawking & Ellis 1973). The outgoing null vector k^μ can be expressed as $k^\mu = (n^\mu + s^\mu)/\sqrt{2}$, where n^μ is unit normal of the spacelike hypersurface defined as $n^\mu = (-\alpha, 0, 0, 0)$, s^μ is the out-directed spacelike vector orthogonal to the surface. The projection tensor $h_{\mu\nu}$ and the extrinsic curvature K_{ij} are described as

$$h_{\mu\nu} = g_{\mu\nu} + n_\mu n_\nu, \quad (\text{A15})$$

$$K_{ij} = h_i^\mu h_j^\nu \nabla_\mu n_\nu. \quad (\text{A16})$$

The expansion Θ is then written as

$$\Theta \equiv \nabla_\mu k^\mu = \nabla_i s^i + K_{ij} s^i s^j - K. \quad (\text{A17})$$

For spherically symmetric spacetime, we can choose the spacelike vector s^i as $s^i = (\psi^{-2}, 0, 0)$, and then the radius r_{AH} of an apparent horizon satisfies the following equation,

$$1 + 2r \frac{\psi_{,r}}{\psi} + \frac{1}{2} r \psi^2 K_r^r \Big|_{r=r_{\text{AH}}} = 0. \quad (\text{A18})$$

Note that an event horizon always lies outside an apparent horizon, and both horizons coincide with each other when the spacetime is stationary. Also an event horizon always forms before the time that an apparent horizon does (Hawking & Ellis 1973).

CONSTRUCTION OF RELATIVISTIC ROTATING EQUILIBRIUM STARS

Here we summarize our method to construct rotating relativistic equilibrium stars, which is based on Komatsu, Eriguchi, & Hachisu (1989); Cook, Shapiro, & Teukolsky (1992, 1994) (see also Stergioulas 2003, for a historical review).

First we focus on how to solve the relativistic Euler equation. The equation can be described in axisymmetric spacetime as

$$\frac{h_{,j}}{h} - \frac{u_{,j}^t}{u^t} + u^t u_\varphi \Omega_{,j} = 0, \quad (\text{B1})$$

where $h \equiv (1 + \varepsilon + P/\rho_0)$ is a specific enthalpy. We also assume specific type of rotation law as

$$u^t u_\varphi = A^2 (\Omega_c - \Omega), \quad (\text{B2})$$

where Ω_c is the central angular velocity, in order to integrate eq. (B1). The Bernoulli's equation is driven by integrating the relativistic Euler equation (B1) as

$$H - K + R = C, \quad (\text{B3})$$

where

$$H \equiv \int \frac{dh}{h} = \ln h = \ln[1 + (n+1)q], \quad (\text{B4})$$

$$K \equiv \int \frac{du^t}{u^t} = \ln u^t = -\frac{1}{2} \ln[\alpha^2 - \psi^4[(\beta^x - \Omega y)^2 + (\beta^y + \Omega x)^2]], \quad (\text{B5})$$

$$R \equiv \int u^t u_\varphi d\Omega = -\frac{1}{2} A^2 (\Omega_c - \Omega)^2, \quad (\text{B6})$$

where $q \equiv P/\rho_0^4$. Note that we have already assumed polytropic equation of state $P = \rho_0^\Gamma$ where $\Gamma = 1 + 1/n$, n is a polytropic index. Therefore, we can describe the matter distribution equation by using eq. (B3) and the rotation law (eq. [B2]) as

$$\begin{aligned} q &= \frac{1}{n+1} \left[\frac{C \exp[A^2(\Omega_c - \Omega)^2/2]}{\sqrt{u^t}} - 1 \right] \\ &= \frac{1}{n+1} \left[\frac{C \exp[A^2(\Omega_c - \Omega)^2/2]}{\sqrt{\alpha^2 - \psi^4[(\beta^x - \Omega y)^2 + (\beta^y + \Omega x)^2]}} - 1 \right], \end{aligned} \quad (\text{B7})$$

$$A^2 (\Omega_c - \Omega) = u^t u_\varphi = \frac{\psi^4 [x(\beta^y + \Omega x) - y(\beta^x - \Omega y)]}{\alpha^2 - \psi^4 [(\beta^x - \Omega y)^2 + (\beta^y + \Omega x)^2]}. \quad (\text{B8})$$

⁴ We only use $q \equiv P/\rho_0$ in this section.

Note that we assume conformally flat spacetime to derive the final part of the equality in eqs. (B7) and (B8).

From the computational point of view, we introduce nondimensional quantities rescaled in the equatorial proper radius of the star (R_e) as

$$\begin{aligned}\hat{x} &= x/R_e, & \hat{y} &= y/R_e, & \hat{z} &= z/R_e, \\ \hat{\Omega} &= R_e\Omega, & \hat{A} &= A/R_e, & \hat{\Delta} &= R_e^2\Delta.\end{aligned}\tag{B9}$$

We also rescale the lapse and conformal factor using the nature of scale free in Newtonian gravity as

$$\hat{\alpha} = \alpha^{1/R_e^2}, \hat{\psi} = \psi^{-1/(2/R_e^2)}.\tag{B10}$$

To determine the matter distribution and rotation profile of the next iteration step, we have to determine five unknown variables (R_e , C , Ω_c , Ω_e , Ω_{\max}) from five equations. Therefore, we evaluate eqs. (B7) and (B8) at three locations, the point of the maximum rest mass density, that of polar surface, and that of the equatorial surface. Note that eq. (B8) becomes an identity at polar surface of the star, and thus we have five equations to be solved. We use Newton-Rapson method (Press et al. 1992) to solve these equations. Once we determine 5 unknown variables, we solve eq. (B8) using Newton-Rapson method to determine the rotation profile. After that we can determine the matter distribution (eq. [B7]).

Next we briefly summarize the gravitational field equations normalized by proper radius as follows.

$$\hat{\Delta}B_i = 8\pi R_e^2 \psi^6 J_i \equiv 4\pi S_{B_i},\tag{B11}$$

$$\hat{\Delta}\chi = -8\pi R_e^2 \psi^6 J_i x^i \equiv 4\pi S_\chi,\tag{B12}$$

$$\hat{\Delta}\psi = -2\pi R_e^2 \psi^5 \rho_H - \frac{1}{8}\psi^{-7} \hat{A}_{ij} \hat{A}^{ij} \equiv 4\pi S_\psi,\tag{B13}$$

$$\hat{\Delta}(\alpha\psi) = 2\pi R_e^2 \alpha\psi(\rho_H + 2S) + \frac{7}{8}\alpha\psi^{-7} \hat{A}_{ij} \hat{A}^{ij} \equiv 4\pi S_{\alpha\psi},\tag{B14}$$

$$\hat{\Delta}P_i = 4\pi R_e^2 \alpha \hat{J}_i \equiv 4\pi S_{P_i},\tag{B15}$$

$$\hat{\Delta}\eta = -4\pi R_e^2 \alpha \hat{J}_i x^i \equiv 4\pi S_\eta.\tag{B16}$$

We choose the same boundary conditions as we choose in our evolution code (see § 2). Note that we construct the star in 3D using octant symmetry to adopt our initial data to our 3D evolution code smoothly.

To summarize, we first solve the gravitational field equations (eqs. [B11] – [B16]). Next, we determine 5 unknown quantities (R_e , C , Ω_c , Ω_e , Ω_{\max}) from 5 equations (eqs. [B7] and [B8]) using Newton-Rapson method. Finally we determine the matter distribution and rotation profile for the next iteration step. We continue this iteration cycle till R_e converges; i.e. R_e goes bellow the error of 10^{-5} . We also check the error rate of physical quantities such as M and J and find that they are in fact below the error rate of 10^{-4} .

REFERENCES

- Baumgarte, T. W. & Shapiro, S. L. 1999, *ApJ*, 526, 941
 Blanchet, L., Damour, T. & Schäfer, G. 1989, *MNRAS*, 242, 289
 Bonazzola, S., Friebe, J., & Gourgoulhon, E. 1998, *A&A*, 331, 280
 Bowers, R. L., & Wilson, J. R. 1991, *Numerical Modeling in Applied Physics and Astrophysics* (Boston: Jones and Bartlett Pub.), Chap. 9.
 Centrella, J. M., New, K. C. B., Lowe, L. L., & Brown, J. D. 2001, *ApJ*, 550, L193
 Chandrasekhar, S. 1965, *ApJ*, 142, 1488
 —. 1969, *Ellipsoidal Figures of Equilibrium*, (New York: Yale Univ. Press), 61
 Chandrasekhar, S. & Lebovitz, N. R. 1965, *ApJ*, 142, 1488
 Cook, G. B., Shapiro, S. L., & Teukolsky, S. A. 1992, *ApJ*, 398, 203
 —. 1994, *ApJ*, 422, 227
 Duez, M., Shapiro, S. L., & Yo, H. -J. 2004, *Phys. Rev. D*, 69, 104016
 Hawking, S. W., & Ellis, G. F. R. 1973, *The large scale structure of space-time*, Chap. 9.2
 Hawley, J. F., Smarr, L. L., & Wilson, J. R. 1984, *ApJS*, 55, 211
 Isenberg, J., & Nester, J. 1980, in *General Relativity and Gravitation Vol. 1: one hundred years after the birth of Albert Einstein*, ed. A. Held (New York: Plenum Press), 23
 Komatsu, H., Eriguchi, Y., & Hachisu, I. 1989, *MNRAS*, 237, 355
 Kormendy, J. 2004, in *Carnegie Observatories Centennial Symposium. 1: Coevolution of Black Holes and Galaxies*, ed. L. C. Ho (Cambridge: Cambridge Univ. Press), in press (astro-ph/0306353)
 Loeb, A., & Rasio, F. A. 1994, *ApJ*, 432, 52
 Leaver, E. W. 1985, *Proc. R. Soc. London A*, 402, 285
 Murata, K., Natori, R. & Karaki, Y. 1990, *Large-scale numerical simulation* (Tokyo: Iwanami), Chap. 5.3 (in Japanese)
 Nakamura, T. 1981, *Prog. Theor. Phys.*, 65, 1876
 Nakamura, T., Oohara, K., & Kojima, Y. 1987, *Prog. Theor. Phys. Suppl.*, 90, Part I, Sec. 2
 Nakamura, T., Shapiro, S. L., & Teukolsky, S. A. 1988, *Phys. Rev. D*, 38, 2972
 New, K. C. B. 2003, *Living Reviews in Relativity*, 6, 2
 New, K. C. B., & Shapiro, S. L. 2001, *ApJ*, 548, 439
 Oohara, K., & Nakamura, T. 1989, *Prog. Theor. Phys.*, 82, 535
 Press, W. H., Flannery, B. P., Teukolsky, S. A., & Vetterling, W. T. 1992, *Numerical Recipes in Fortran* (2nd ed.; Cambridge: Cambridge Univ. Press), Chap. 9.6
 Rees, M. J. 1998, in *Black Holes and Relativistic Stars*, ed. R. M. Wald (Chicago: Univ. Chicago Press), 79
 —. 2001, in *Black Holes in Binaries and Galactic Nuclei*, ed. L. Kaper, E. P. J. van den Heuvel, & P. A. Woudt (New York: Springer-Verlag), 351
 Ruffert, M. 1992, *A&A*, 265, 82
 Saijo, M., Shibata, M., Baumgarte, T. W., & Shapiro, S. L. 2001, *ApJ*, 548, 919
 Saijo, M., Baumgarte, T. W., Shapiro, S. L., & Shibata, M. 2002, *ApJ*, 569, 349
 Saijo, M., Baumgarte, T. W., & Shapiro, S. L. 2003, *ApJ*, 595, 352
 Sekiguchi, Y. -I., & Shibata, M. 2004, *Phys. Rev. D*, submitted (gr-qc/0403036)
 Shapiro, S. L. & Teukolsky, S. A. 1980, *ApJ*, 235, 199
 —. 1983, *Black Holes, White Dwarfs and Neutron Stars*, (New York: John Wiley and Sons), Chap. 7
 —. 1985, *ApJ*, 298, 34
 —. 1991, *Phys. Rev. Lett.*, 66, 994
 —. 1992, *Phys. Rev. D*, 54, 2006
 Shibata, M. 1997, *Phys. Rev. D*, 55, 2002
 —. 2000, *Prog. Theor. Phys.*, 104, 325

- . 2003, *ApJ*, 595, 992
- . 2004, *ApJ*, 605, 350
- Shibata, M., Baumgarte, T. W., & Shapiro, S. L. 2000, *ApJ*, 542, 453
- Shibata, M & Nakamura, T. 1995, *Phys. Rev. D*, 52, 5428
- Shibata, M & Shapiro, S. L. 2002, *ApJ*, 572, L39
- Stark, R. F. & Piran, T. 1985, *Phys. Rev. Lett.*, 55, 891 (erratum 56, 97)
- . 1986, in *Dynamical Spacetimes and Numerical Relativity*, ed. J. M. Centrella (Cambridge: Cambridge Univ. Press), 40
- Sterioulas, N. 2003, *Living Reviews in Relativity*, 6, 3
- Thorne, K. S. 1998, in *Black Holes and Relativistic Stars*, ed. R. M. Wald (Chicago: Univ. Chicago Press), 41
- van Leer, B. 1977, *J. Comp. Phys.*, 23, 276
- Wald, R. M. 1984, *General Relativity* (Chicago: Univ. Chicago Press), Chap. 12.1
- Wilson, J. R. 1979, in *Sources of Gravitational Waves*, ed. L. L. Smarr (Cambridge: Cambridge Univ. Press), 423
- Wilson, J. R. & Mathews, G. J. 1989, in *frontiers in numerical relativity*, ed. C. R. Evans, L. S. Finn, D. W. Hobill (Cambridge: Cambridge Univ. Press), 306
- . 1995, *Phys. Rev. Lett.*, 75, 4161
- York, J. W., Jr. 1979, in *Sources of Gravitational Waves*, ed. L. L. Smarr (Cambridge: Cambridge Univ. Press), 83